Available online at www.sciencedirect.com
SCIENCE DIRECT®
Optics Communications 244 (2005) 233–243
OPTICS COMMUNICATIONS
www.elsevier.com/locate/optcom

Analysis of apodized phase-shifted long-period fiber gratings

Florence Y.M. Chan, K.S. Chiang *

Optoelectronics Research Centre and Department of Electronic Engineering, City University of Hong Kong, 83 Tat Chee Avenue, Hong Kong, China

Received 9 April 2004; received in revised form 9 September 2004; accepted 22 September 2004

Abstract

We present a detailed theoretical analysis of the transmission spectra of apodized phase-shifted long-period fiber gratings (LPFGs). Simple analytical formulas are derived to provide insights into the characteristics of the gratings and facilitate their designs for specific applications. In particular, we focus on the achievement of zero or complete transmission at the resonance wavelength with zero- or π-phase-shifted gratings. The effects of index apodization and length apodization on the transmission spectra of the LPFGs are studied in detail. A number of numerical examples are given to illustrate the features of various kinds of LPFG designs.

Keywords: Coupled-mode theory; Long-period fiber gratings; Apodized gratings; Phase-shifted gratings; Optical filters; Wavelength-division multiplexers

1. Introduction

Long-period fiber grating (LPFG), which is produced by introduction of a periodic modulation of the refractive index in the core of a single-mode fiber, has generated tremendous interest in the fields of optical communications and optical sensing. An LPFG allows light coupling between the guided mode and the cladding modes, which results in a series of attenuation bands centered at discrete wavelengths in the transmission spectrum [1]. LPFGs have been developed into many useful components, including gain flattening filters for erbium-doped fiber amplifiers [2–8], dispersion compensators [9–11], widely tunable filters [12,13], and broadband add/drop multiplexers [14,15], as well as a wide range of optical sensors [16–18]. A distinct feature of LPFGs is their flexibility in achieving desired transmission characteristics by variation of the grating parameters (e.g., index modulation, grating period, grating length, chirping, phase shifts, etc.). For example, index apodization has been used for the elimination of side lobes in the transmission spectrum [19] and phase

* Corresponding author. Tel.: +852 27889605; fax: +852 27887791.
E-mail address: eeksc@cityu.edu.hk (K.S. Chiang).

0030-4018/$ - see front matter © 2004 Elsevier B.V. All rights reserved.
doi:10.1016/j.optcom.2004.09.078

shifts have been introduced along an LPFG for the generation of narrow passing bands [20,21]. Flat-top band-pass filters [22] and band-rejection filters [23] have also been demonstrated with LPFGs consisting of multiple phase shifts.

In this paper, we present a detailed theoretical analysis of apodized phase-shifted LPFGs using the transfer matrix method. The general conditions for achieving zero or complete transmission at the resonance wavelength are derived. The effects of index apodization and length apodization on the transmission spectrum are discussed. Numerical examples are given for the design of band-pass, band-rejection, and comb filters. Our study provides a better understanding of the characteristics of LPFGs, which should facilitate the design of LPFG-based devices.

2. Method of analysis

We consider an LPFG consisting of M sections, as shown in Fig. 1, where φ is the phase shift between two adjacent sections. The grating pitch Λ is the same in all sections, but the amplitude of the index modulation and the length are allowed to vary from section to section. The resonance wavelength of the LPFG, λ_0, is determined by the phase-matching condition [1]

$$\lambda_0 = (N_{01} - N_{0m})\Lambda, \tag{1}$$

where N_{01} and N_{0m} are the effective indices of the LP_{01} and LP_{0m} ($m = 2,3,4,\ldots$) modes, respectively. For a sinusoidal index modulation along the direction of wave propagation z, the coupled-mode equations for the ith section of the grating that describe the coupling of the amplitudes of the LP_{01} and LP_{0m} modes, $A(z)$ and $B(z)$, are given by [21]

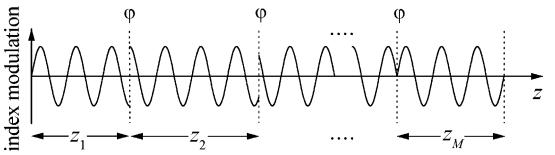

Fig. 1. Schematic diagram of a phase-shifted multi-section LPFG.

$$\frac{dA}{dz} = \kappa_i B e^{j2\delta z} e^{-j\varphi_i}, \tag{2}$$

$$\frac{dB}{dz} = -\kappa_i A e^{-j2\delta z} e^{j\varphi_i}, \tag{3}$$

where

$$\delta = \frac{\pi}{\Lambda}\left(\frac{\lambda_0}{\lambda} - 1\right) \tag{4}$$

is the phase mismatch, which is a measure of the deviation of the operating wavelength λ from the resonance wavelength λ_0. κ_i is the coupling coefficient (a real positive number), which is proportional to the amplitude of the index modulation and the overlapping between the LP_{01} and LP_{0m} mode fields over the cross-sectional area of the fiber core (assuming index modulation in the fiber core only). φ_i is the initial phase of the ith section. The electric fields of the LP_{01} and LP_{0m} modes, $E_A(z)$ and $E_B(z)$, are related to their amplitudes by $E_A(z) = A(z)e^{-j\beta_{01}z}$, and $E_B(z) = B(z)e^{-j\beta_{0m}z}$, respectively, where β_{01} and β_{0m} are the corresponding propagation constants. Each section of the LPFG can be represented by a transfer matrix that relates the input and output electric fields of the modes [21]. Therefore, the output electric fields from the LPFG can be obtained by simply multiplying the transfer matrices of all sections [21]:

$$\begin{pmatrix} E_A(L) \\ E_B(L) \end{pmatrix} = F_M \cdots F_3 F_2 F_1 \begin{pmatrix} E_A(0) \\ E_B(0) \end{pmatrix}, \tag{5}$$

where

$$F_i = \begin{pmatrix} e^{-j(\beta_{01}-\delta)z_i} & 0 \\ 0 & e^{-j(\beta_{0m}+\delta)z_i} \end{pmatrix} \times \begin{pmatrix} \cos(Q_i z_i) - j\frac{\delta}{Q_i}\sin(Q_i z_i) & \frac{\kappa_i}{Q_i}e^{-j\varphi_i}\sin(Q_i z_i) \\ -\frac{\kappa_i}{Q_i}e^{j\varphi_i}\sin(Q_i z_i) & \cos(Q_i z_i) + j\frac{\delta}{Q_i}\sin(Q_i z_i) \end{pmatrix} \tag{6}$$

is the transfer matrix for the ith section, z_i is the corresponding section length, $Q_i = (\delta^2 + \kappa_i^2)^{1/2}$, $L = \sum_{j=1}^{i=m} z_i$ is the total length of the LPFG, and the initial phase is given by

$$\phi_i = \frac{2\pi}{\Lambda}\sum_{j=1}^{j=i-1} z_j + (i-1)\varphi. \tag{7}$$

While the above formulation is general, we limit our study to the more popular cases $\varphi = 0$ and $\varphi = \pi$, which produce symmetric transmission spectra. With light launched only into the LP_{01} mode, i.e., $E_A(0) = 1$ and $E_B(0) = 0$, the normalized output of the LP_{01} mode at the resonance wavelength (i.e., at $\delta = 0$) is obtained as

$$|E_A(L)|^2 = \cos^2\left(\sum_{i=1}^{i=M} \kappa_i z_i\right) \tag{8}$$

for $\varphi = 0$, or

$$|E_A(L)|^2 = \cos^2\left[\sum_{i=1}^{i=M} (-1)^i \kappa_i z_i\right] \tag{9}$$

for $\varphi = \pi$. Eq. (8) implies that the transmission at the resonance wavelength remains unchanged when the sum of $\kappa_i z_i$ over all sections does not change. Eq. (9) has a similar interpretation, except for the alternating signs arising from the π-phase shifts. These two equations can be regarded as conservation laws for these special multi-section LPFGs, which show readily how the coupling coefficients κ_i and the section lengths z_i should be chosen to produce desirable transmission at the resonance wavelength. In many practical situations, we are interested in the two extreme cases: zero transmission with $|E_A(L)|^2 = 0$ and complete transmission with $|E_A(L)|^2 = 1$. According to Eqs. (8) and (9), the conditions for zero transmission are

$$\sum_{i=1}^{i=M} \kappa_i z_i = \frac{\pi}{2}(1 + 2n) \quad \text{for} \quad \varphi = 0, \tag{10}$$

$$\sum_{i=1}^{i=M} (-1)^i \kappa_i z_i = \pm\frac{\pi}{2}(1 + 2n) \quad \text{for} \quad \varphi = \pi, \tag{11}$$

and those for complete transmission are

$$\sum_{i=1}^{i=M} \kappa_i z_i = (1 + n)\pi \quad \text{for} \quad \varphi = 0, \tag{12}$$

$$\sum_{i=1}^{i=M} (-1)^i \kappa_i z_i = \pm n\pi \quad \text{for} \quad \varphi = \pi, \tag{13}$$

where n (= 0, 1, 2, 3,....) arises from the fact that the output at δ=0 varies sinusoidally with $\sum \kappa_i z_i$ or $\sum (-1)^i \kappa_i z_i$. The design of an LPFG filter relies on the control of the coupling coefficients and the section lengths. The technique of using equal section lengths and different coupling coefficients is referred to as index apodization (since the coupling coefficient is proportional to the magnitude of the index modulation), while the technique of using equal coupling coefficients and different section lengths (with phase shifts) is referred to as length apodization [21].

For the simulation work given in the subsequent sections, we assume that the fiber has a core index of $n_1 = 1.4486$ and a cladding index of $n_2 = 1.4408$. Other parameters used in the calculations are: core radius $a = 3.6$ μm, cladding radius $\rho = 62.5$ μm, $\Lambda = 200.0$ μm, surrounding index $n_3 = 1$ (air), and cladding mode order $m = 8$. With these parameters, the resonance wavelength λ_0 is fixed at 1.550 μm. Unless stated otherwise, the total length of the grating is $L = 40$ mm.

3. A single uniform LPFG ($M = 1$)

We first study the simplest case $M = 1$ (i.e., a single uniform LPFG) to provide a reference for more complicated cases. From Eq. (10), we obtain the well-known formula for the design of a band-rejection LPFG filter:

$$\kappa = \frac{\pi}{2L}(1 + 2n), \quad n = 0, 1, 2, 3, \ldots \tag{14}$$

The complete transmission spectrum can be found readily from Eqs. (5) and (6):

$$|E_A(L)|^2 = \cos^2\left[L(\delta^2 + \kappa^2)^{1/2}\right] + \frac{\delta^2}{\delta^2 + \kappa^2}\sin^2\left[L(\delta^2 + \kappa^2)^{1/2}\right]. \tag{15}$$

In general, the spectrum consists of a rejection band centered at the resonance wavelength and a series of side lobes defined by specific locations with 100% transmission, as shown in Fig. 2(a). From Eqs. (14) and (15), the locations that define the side lobes are obtained as

$$\delta_{\pm p} = \mp\frac{\pi}{2L}\left[4p^2 - (1 + 2n)^2\right]^{1/2}, \tag{16}$$

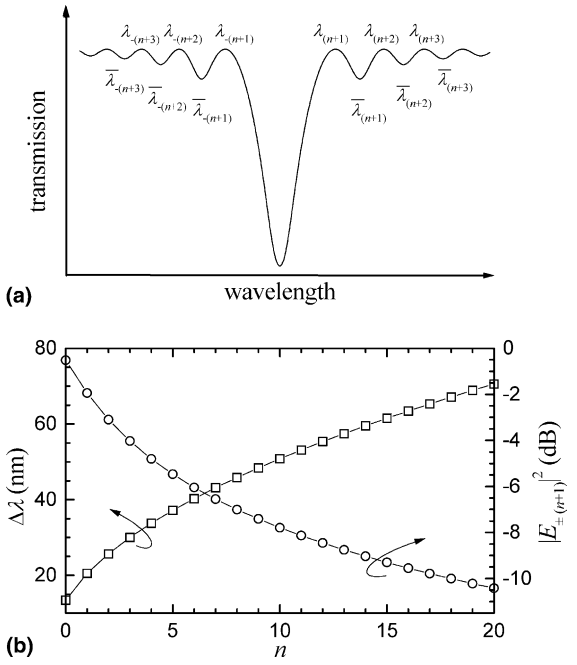

Fig. 2. (a) Transmission spectrum of a uniform LPFG defining the locations of the maxima and the minima. (b) Variations of the bandwidth and the contrast of the first side lobe with n for a uniform LPFG.

where $p = n+1, n+2,\ldots$ The corresponding wavelengths are given by

$$\lambda_{\pm p} = \frac{\lambda_0}{1 \mp \frac{\Lambda}{2L}\left[4p^2 - (1+2n)^2\right]^{1/2}}. \tag{17}$$

The wavelength span of the rejection band is thus given by $\Delta\lambda = \lambda_{+(n+1)} - \lambda_{-(n+1)}$, i.e.,

$$\Delta\lambda = \frac{\lambda_0 \Lambda}{L}(4n+3)^{1/2}, \tag{18}$$

which shows explicitly how the bandwidth of the rejection band increases with n and inversely with the grating length L. To locate the side lobes, we look for the conditions that satisfy $\mathrm{d}|E_A|^2/\mathrm{d}\delta = 0$ from Eq. (15) and find

$$\overline{\delta}_{\pm p} = \mp\frac{1}{L}\left\{x_p^2 - \left[\frac{\pi}{2}(1+2n)\right]^2\right\}^{1/2}, \tag{19}$$

where $p = n+1, n+2,\ldots$ and x_p are the roots of the equation $\tan(x_p) = x_p$, which approaches $\pi(1+2p)/2$ as p increases. With the help of a highly accurate approximate formula [24] for x_p:

$$x_p = \frac{\pi(1+2p)}{2} - \frac{2}{\pi(1+2p)}, \tag{20}$$

the locations of all the side lobes can be calculated explicitly:

$$\overline{\delta}_{\pm p} = \mp\frac{\pi}{L}[(1+p+n)(p-n)]^{1/2} \times \left[1 - \frac{1}{\pi^2(1+p+n)(p-n)}\right], \tag{21}$$

$$\overline{\lambda}_{\pm p} = \frac{\lambda_0}{\overline{\delta}_{\mp p}\Lambda/\pi + 1}. \tag{22}$$

The transmission of the side lobe at $\overline{\lambda}_{\pm p}$ is simply given by

$$\left|\overline{E}_{\pm p}\right|^2 = 1 - \left(\frac{1+2n}{1+2p}\right)^2. \tag{23}$$

Eqs. (19)–(23) are convenient formulas for the evaluation of the side lobes, which, surprisingly, have not been reported previously, regardless of the large amount of published work on a single uniform LPFG.

The variations of the bandwidth and the size of the first side lobe (i.e., $p = n+1$) with n are shown in Fig. 2(b). Although an infinite number of κ (corresponding to $n = 0, 1, 2,\ldots$), as given by Eq. (14), is allowed, the side lobes in the transmission spectrum become more and more significant as n and hence κ becomes larger and larger, as shown by Eq. (23). While the bandwidth of the filter can be increased effectively by using a large coupling coefficient, the significance of the side lobes is also increased accordingly. Apodization can overcome this limitation.

4. Index apodization

Index apodization refers to the use of different coupling coefficients in different sections of a multi-section LPFG, so it applies to both $\varphi = 0$ and $\varphi = \pi$.

4.1. Zero transmission at λ_0 with $M > 1$ and $\varphi = 0$

For M equal-length sections with $\varphi = 0$, Eq. (10) gives the condition:

$$\sum_{i=1}^{i=M} \kappa_i = M\pi(1+2n)/(2L), \tag{24}$$

which guarantees 100% rejection at λ_0.

We consider a Gaussian index apodization profile described by

$$\kappa_i = \frac{M\pi(1+2n)}{2L} \times \frac{f_i}{\sum_{i=1}^{i=M} f_i}, \tag{25}$$

where

$$f_i = \exp\left[-\ln(2)\left(\frac{2i-M-1}{Mw}\right)^2\right] \tag{26}$$

and w is its full-width at half maximum (FWHM). The transmission spectra calculated for $M = 18$ with $w = 0.8$, 0.5 and 0.3 are shown in Fig. 3(a) for two cases: $n = 0$ and $n = 5$, where the spectra of a uniform LPFG of the same length with $\kappa = 39.27\ \text{m}^{-1}$ ($n = 0$) and $\kappa = 431.97\ \text{m}^{-1}$ ($n = 5$), respectively, are also shown for comparison. For $n = 0$, the bandwidth, the positions of the most significant side lobes, and the corresponding transmission for the uniform LPFG are 13.4 nm, 1.540 μm and 1.560 μm, and –0.51 dB, respectively, while, for $n = 5$, the corresponding values are 37.1 nm, 1.524 μm and 1.577 μm, and –5.47 dB, respectively. The change of the contrast of the most significant side lobes with w is shown in Fig. 3(b). It can be seen that the side lobes can be suppressed effectively with a Gaussian index apodization profile. Furthermore, apodization tends to smooth the rejection band. To limit the contrast of the side lobes to less than 0.1 dB, w must be smaller than 0.79 for $n = 0$ and 0.48 for $n = 5$. The effects of the section number M on the transmission spectra have also been studied. As M increases, the most significant side lobes shift away from the rejection band and their contrast is reduced. The change of the contrast of the most significant side lobes with M is shown in Fig. 4 for $w = 0.5$ and $n = 0$. We need at least six sections to limit the contrast of the side lobes to less than 0.1 dB.

For the suppression of side lobes, we should use symmetric apodization profiles with a maximum value of κ_i in the middle. We have studied various profile shapes, including Gaussian, sine, parabolic, and triangular profiles, and found that the Gaussian profile gives the best results. On the other hand, symmetric apodization profiles with a minimum value of κ_i in the middle result in large, closely packed side lobes. A binary apodization profile (namely, a profile that allows only two values for the coupling coefficients) with a zero

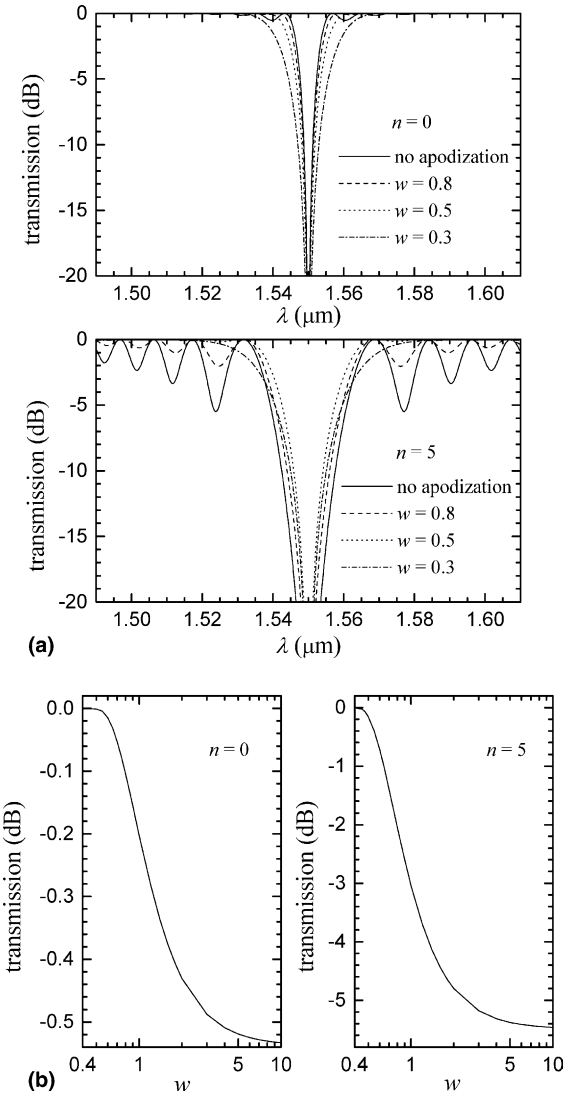

Fig. 3. (a) Transmission spectra of Gaussian index apodized LPFGs with $\varphi = 0$ and $M = 18$ for $w = 0.8$, 0.5 and 0.3, and a uniform LPFG of the same length with $\kappa = 431.97\ \text{m}^{-1}$, which guarantee complete rejection at $\lambda_0 = 1550$ nm. (b) Variation of the contrast of the first side lobe with w for $n = 0$ and $n = 5$.

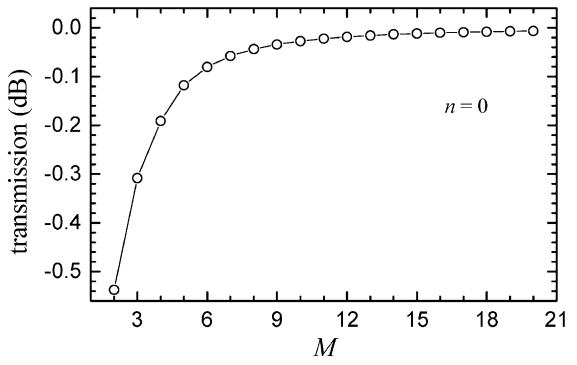

Fig. 4. Variation of the contrast of the first side lobe with M for the Gaussian index apodized LPFG with $w = 0.5$ for $n = 0$.

coupling coefficient in the middle can enhance such a feature and result in a comb filter. As an example, we analyze a binary index apodization profile with $\kappa_1 = \kappa_M$ and $\kappa_i = 0$ for $i = 2, 3, \ldots, M-1$. The initial phase for the last section is given by Eq. (7) using $\varphi = 0$. This composite grating is equivalent to a three-section profile with $\kappa_1 = \kappa_3$, $\kappa_2 = 0$, $z_1 = z_3 = L/M$, and $z_2 = (M-2)L/M$, i.e, two uniform LPFGs of equal lengths separated by the distance z_2. According to Eq. (24), the coupling coefficients are given by

$$\kappa_1 = \kappa_3 = \pi(1+2n)/(4z_1). \tag{27}$$

The transmission spectrum of this LPFG is obtained as

$$|E_A(L)|^2 = 1 - \left[2\left(\frac{\kappa_1}{Q_1}\right)\sin(Q_1 z_1)\cos(Q_1 z_1)\cos(\delta z_2) - 2\left(\frac{\kappa_1}{Q_1}\right)\left(\frac{\delta}{Q_1}\right)\sin^2(Q_1 z_1)\sin(\delta z_2)\right]^2 \tag{28}$$

With $\kappa_1 \gg \delta$, the locations of the maxima in the transmission spectrum are found as

$$\delta_{\pm q} = \mp\frac{\pi}{2z_2}(1+2q), \quad q = 0, 1, 2, 3, \ldots \tag{29}$$

The corresponding wavelengths are

$$\lambda_{\pm q} = \frac{\lambda_0}{1 \mp \frac{\Lambda}{2z_2}(1+2q)}, \tag{30}$$

which implies that the pass bands are equally spaced (i.e., a transmission spectrum of a comb filter) with a spacing given by

$$\Delta\lambda = \lambda_0 \Lambda / z_2. \tag{31}$$

Clearly, the channel spacing can be adjusted by simply changing the length z_2. To obtain a spacing of 20 nm for CWDM applications, the length z_2 required is 15 mm. To obtain a spacing of 0.8 nm for DWDM applications, however, the length z_2 must be increased to 387 mm. The transmission spectra for three cases, (i) $z_1 = 3$ mm, $z_2 = 15$ mm, and $n = 0$ ($L = 21$ mm, $M = 7$, and $\kappa_1 = 261.80$ m^{-1}), (ii) $z_1 = 3$ mm, $z_2 = 387$ mm, and $n = 0$ ($L = 393$ mm, $M = 131$, and $\kappa_1 = 261.80$ m^{-1}), and (iii) $z_1 = 9$ mm, $z_2 = 387$ mm, and $n = 0$ ($L = 405$ mm, $M = 45$, and $\kappa_1 = 87.27$ m^{-1}), are shown in Fig. 5(a). In general, the span of the channels decreases with an increase in z_1. Our analysis agrees with the experimental results reported elsewhere [25–29]. By adjusting the value of κ_1 slightly (i.e., by relaxing the condition for zero transmission at λ_0 slightly), the difference of the contrasts between the channels can be significantly reduced, as shown in Fig. 5(b), where κ_1 is increased from 261.80 to 272.27 m^{-1} and from 87.27 to 91.19 m^{-1} for the respective cases shown in Fig. 5(a). Previous works on comb filters [26–28] have emphasized mainly on the determination of wavelength spacing. Our results, Eqs. (27)–(30), give more details on the design parameters and the transmission characteristics of the filter.

To demonstrate the effects of an asymmetric apodization profile, Fig. 6 shows the transmission spectrum of an LPFG with a half Gaussian profile (for $M = 18$, $w = 0.5$, and $n = 5$). As shown in Fig. 6, a significant pedestal is present in the spectrum, which is typical of an asymmetric apodization profile. In fact, such a pedestal has been observed experimentally with an asymmetric step apodization profile [30].

4.2. Zero transmission at λ_0 with $M > 1$ and $\varphi = \pi$

For M (>1) equal-length sections with $\varphi = \pi$, Eq. (11) gives the following condition for the coupling coefficients:

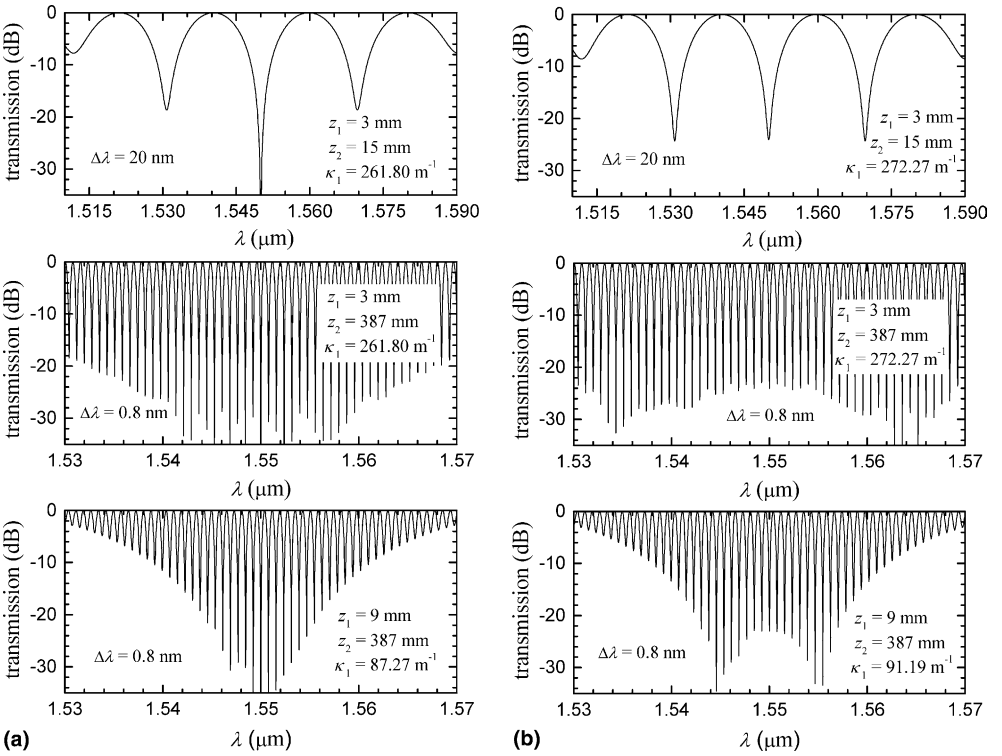

Fig. 5. (a) Transmission spectra of several composite LPFGs, formed by two uniform LPFGs of equal lengths (z_1) separated by a length of fiber (z_2), where zero transmission at $\lambda_0 = 1550$ nm is strictly enforced. (b) Transmission spectra obtained using the same parameters in (a) except that the value of κ_1 is increased slightly to reduce the contrast difference among the channels.

$$\sum_{i=1}^{i=M}(-1)^i\kappa_i = \pm M\pi(1+2n)/(2L), \tag{32}$$

which cannot be satisfied with a symmetric index apodization profile over an even number of sections (because such a profile gives $\sum_{i=1}^{i=M}(-1)^i \kappa_i = 0$.) Here, we use a linear profile to illustrate the features of this class of LPFGs:

$$\kappa_i = \frac{(-1)^M M\pi(1+2n)}{2L} \times \frac{i}{\sum_{j=1}^{j=M}(-1)^j j}. \tag{33}$$

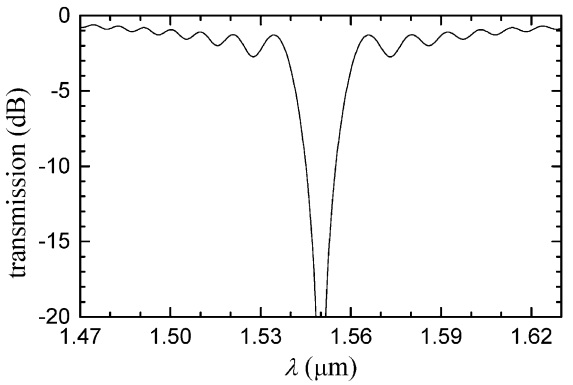

Fig. 6. Transmission spectrum of the half Gaussian index apodized LPFGs with $\varphi = 0$, $n = 5$, $w = 0.5$, and $M = 18$, which guarantees complete rejection at $\lambda_0 = 1550$ nm.

The transmission spectra calculated with $n = 0$ are shown in Fig. 7 for $M = 3$, 15, and 25. As shown in Fig. 7, the LPFG can be designed to operate as a broadband rejection filter with a high extinction ratio and the bandwidth increases with M. However, the coupling coefficients required can become large when M is large. For the examples given in Fig. 7, the highest coupling coefficients required are 176.71, 1104.47, and 1887.98 m^{-1} for $M = 3$, 15, and 25, respectively. For reference, a UV-induced index modulation of 10^{-3} in the fiber core gives a coupling coefficient of $\sim$1000 m^{-1}.

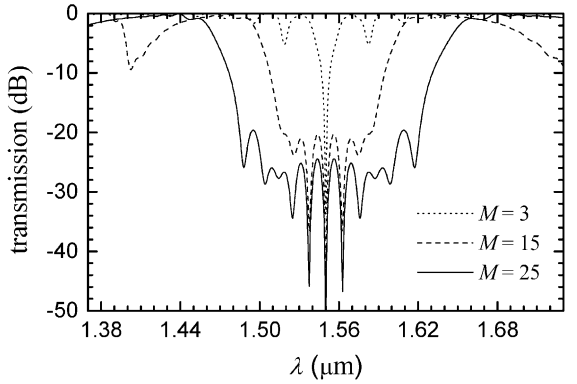

Fig. 7. Transmission spectra of linearly index apodized LPFGs with $\varphi = \pi$ and $n = 0$ for $M = 3$, 15, and 25, which guarantee complete rejection at $\lambda_0 = 1550$ nm.

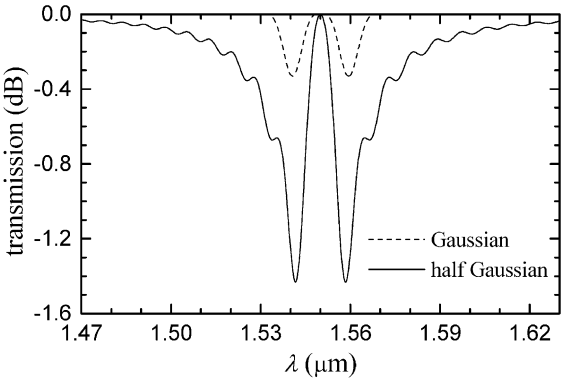

Fig. 8. Transmission spectra of Gaussian and half Gaussian index apodized LPFGs with $\varphi = 0$, $n = 0$, and $M = 18$, which guarantee complete transmission at $\lambda_0 = 1550$ nm.

4.3. Complete transmission at λ_0 with $M > 1$ and $\varphi = 0$

Here, we consider an apodized LPFG without phase shifts that gives complete transmission at λ_0. According to Eq. (12), the condition for the coupling coefficients is

$$\sum_{i=1}^{i=M} \kappa_i = M\pi(1+n)/L. \tag{34}$$

The transmission spectra calculated with $n = 0$ are shown in Fig. 8 for Gaussian and half Gaussian apodization profiles ($M = 18$). As shown in Fig. 8, the contrasts of the spectra are low. These LPFGs do not function as effective band-pass filters, regardless of the fact that complete transmission at λ_0 can be enforced. To operate as a neat band-pass filter, all wavelengths other than those near λ_0 must be rejected, but this function is physically impossible with a single LPFG, which tends to pass light at wavelengths far away from its resonance wavelength.

4.4. Complete transmission at λ_0 with $M > 1$ and $\varphi = \pi$

The condition for achieving complete transmission at λ_0 with M (>1) equal-length sections and $\varphi = \pi$ is given by Eq. (13), namely,

$$\sum_{i=1}^{i=M} (-1)^i \kappa_i = \pm n\pi M/L. \tag{35}$$

With $n = 0$, any symmetric apodization profile over an even number of sections satisfies Eq. (35). We again consider a Gaussian apodization profile:

$$\kappa_i = R\kappa_0 M \times \frac{f_i}{\sum_{i=1}^{i=M} f_i}, \tag{36}$$

where f_i is given by Eq. (26), $\kappa_0 = \pi/2L$ is the minimum value of κ to produce zero transmission at λ_0 for a uniform LPFG, R is a constant, and the average coupling coefficient of the LPFG, $\Sigma\kappa_i/M$, is equal to $R\kappa_0$. It is known that the transmission spectrum of an LPFG consisting of M uniform π-phase-shifted sections contains two sharp rejection bands located symmetrically on both sides of the resonance wavelength with $M - 2$ large ripples in between [21]. Here, we find that the ripples can be eliminated effectively by using the Gaussian index apodization profile given in Eq. (36). As an example, the transmission spectrum for $M = 7$ and $R = 1.54$ is shown in Fig. 9(a), together with that of a uniform seven-section LPFG with $\varphi = \pi$ and $R = 1.56$. As shown in Fig. 9(a), the ripples between the two rejection bands are eliminated almost completely with the index apodization. The transmission of the two rejection bands depends on the value of R and can reach zero when an optimal value of R is used. The optimal value of R, the locations of the rejection bands $\hat{\delta}$, and the wavelength span of the rejection bands $\Delta\hat{\lambda}$ can be found by solving Eq. (5) with $|E_A(L)|^2 = 0$. We find that $\Delta\hat{\lambda}$ increases with n and $\hat{\delta}/\kappa_0$ is proportional

to R, and the side lobes and the ripples also increase with n. In general, $\Delta\hat{\lambda}$ can be expressed as

$$\Delta\hat{\lambda} = \frac{\lambda_0 \Lambda}{L}\left(\frac{|\hat{\delta}|}{\kappa_0}\right). \tag{37}$$

The variations of $|\hat{\delta}|/\kappa_0$ and $\Delta\hat{\lambda}$ with M (for $n = 0$ and using optimal values of R) are presented in Fig. 9(b), which are found to be linear and almost the same for both the Gaussian and uniform profiles.

5. Length apodization

Length apodization applies only to the case $\varphi = \pi$. Discussions of some specific length apodization profiles can be found in [21,22]. Here, we provide more detailed and general results.

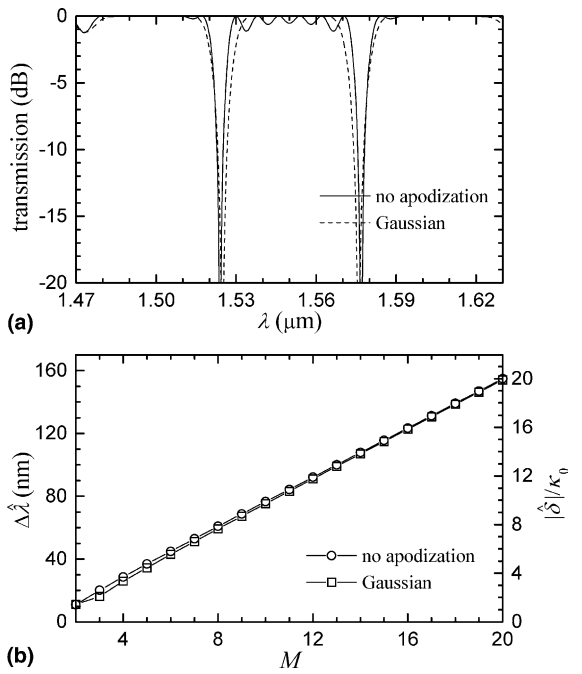

Fig. 9. (a) Transmission spectra of a Gaussian index apodized LPFG with $w = 0.5$ and $R = 1.54$, and a uniform LPFG with $R = 1.56$, showing two distinct rejection bands at both sides of the resonance wavelength. For both LPFGs, $\varphi = \pi$ and $M = 7$. (b) Variations of the value $|\hat{\delta}|/\kappa_0$ and the span of the rejection band $\Delta\hat{\lambda}$ with M for the Gaussian index apodized LPFG with $w = 0.5$ and the uniform LPFG of the same total length. For both LPFGs, $\varphi = \pi$ and $n = 0$.

5.1. Zero transmission at λ_0

To achieve zero transmission at λ_0 with length apodization only, we obtain the following condition from Eq. (11):

$$\sum_{i=1}^{i=M}(-1)^i z_i = \pm\pi(1+2n)/(2\kappa), \tag{38}$$

where κ is the coupling coefficient for all sections. Symmetric length apodization profiles over an even number of sections give $\sum_{i=1}^{i=M}(-1)^i z_i = 0$ and, hence, do not satisfy Eq. (38). Therefore, we use a linear length apodization profile as an example:

$$z_i = \frac{i}{\sum_{j=1}^{j=M} j} \times L. \tag{39}$$

Putting Eq. (39) into Eq. (38), we obtain the coupling coefficient:

$$\kappa = \frac{(-1)^M \pi(1+2n)}{2L} \times \frac{\sum_{i=1}^{i=M} i}{\sum_{i=1}^{i=M}(-1)^i i}. \tag{40}$$

The transmission spectra calculated with $n = 0$ are shown in Fig. 10 for $M = 3$, 15, and 25, which correspond to $\kappa = 117.81$, 589.05, and 981.75 m^{-1}, respectively. A wide rejection band with transmission less than -20 dB can be achieved as M becomes large enough. Compared with the corresponding linear index apodization discussed in Section 4.2 (Fig. 7), the length apodization produces more significant side lobes and less sharp band transitions.

5.2. Complete transmission at λ_0

The condition for the achievement of complete transmission at λ_0 with length apodization is given by Eq. (13) as

$$\sum_{i=1}^{i=M}(-1)^i z_i = \pm n\pi/\kappa, \tag{41}$$

which is satisfied with any symmetric length apodization profile over an even number of sections for $n = 0$. Similar to the corresponding index apodization discussed in Section 4.4, the present case can give rise to two sharp rejection bands located symmetrically on both sides of the resonance

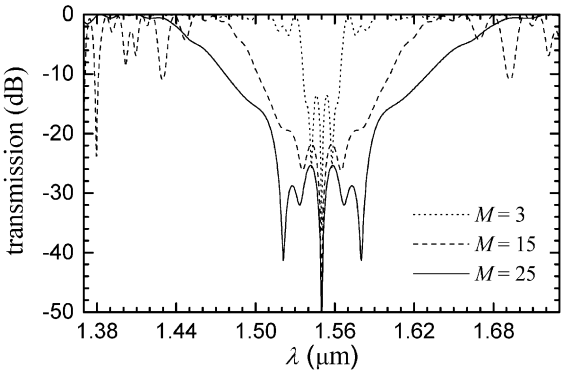

Fig. 10. Transmission spectra of linearly length apodized LPFGs with $\varphi = \pi$ and $n = 0$ for $M = 3$, 15, and 25, which guarantee complete rejection at $\lambda_0 = 1550$ nm.

wavelength. Here, we use a Gaussian length apodization profile as an example:

$$z_i = \frac{f_i}{\sum_{i=1}^{i=M} f_i} \times L, \tag{42}$$

where f_i is given by Eq. (26). The coupling coefficient κ can be expressed as $R\kappa_0$, where $\kappa_0 = \pi/2L$ and R is the value required for the transmission of the two rejection bands to reach zero. The introduction of suitable length apodization is expected to eliminate the ripples between the two rejection bands [21,22]. As an example, the transmission spectrum calculated with $M = 7$ and $R = 2.00$ is shown in Fig. 11(a), together with the spectrum of a uniform seven-section LPFG with $\varphi = \pi$ and $R = 1.56$. As shown in Fig. 11(a), the ripples between the two rejection bands can be eliminated with length apodization, but significant side lobes are generated on the other sides of the rejection bands. We find that the wavelength span of the rejection bands $\Delta\hat{\lambda}$, the side lobes, and the ripples increase with n, and $\Delta\hat{\lambda}$ is proportional to $|\hat{\delta}|/\kappa_0$, where $\hat{\delta}$ gives the location of the rejection band. Fig. 11(b) shows that $|\hat{\delta}|/\kappa_0$ and $\Delta\hat{\lambda}$ vary linearly with M (for $n = 0$). Unlike the results shown in Fig. 9, the wavelength span of the rejection band $\Delta\hat{\lambda}$ depends on the length apodization profile and the slope at the -3 dB point of the rejection band is significantly smaller.

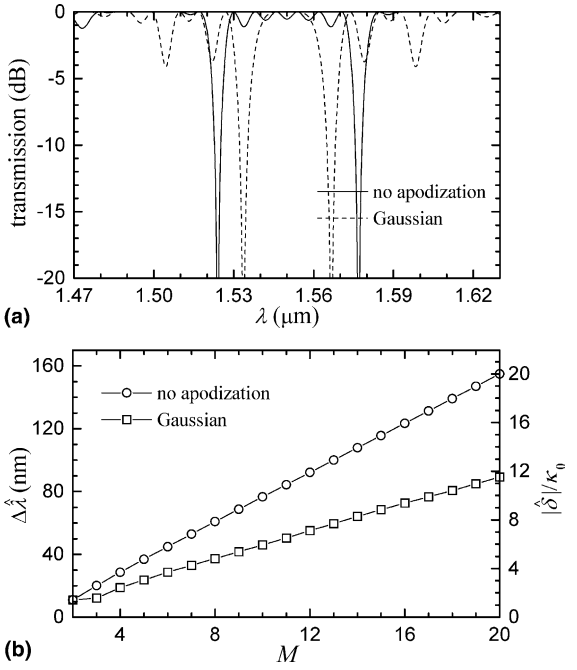

Fig. 11. (a) Transmission spectra of a Gaussian length apodized LPFG with $w = 0.5$ and $R = 2.00$, and a uniform LPFG with $R = 1.56$, showing two distinct rejection bands at both sides of the resonance wavelength. For both LPFGs, $\varphi = \pi$ and $M = 7$. (b) Variations of the value $|\hat{\delta}|/\kappa_0$ and the span of the rejection band $\Delta\hat{\lambda}$ with M for the Gaussian length apodized LPFG with $w = 0.5$ and the uniform LPFG of the same total length. For both LPFGs, $\varphi = \pi$ and $n = 0$.

6. Conclusion

A detailed theoretical study of apodized phase-shifted LPFGs is presented. The conditions for achieving zero and complete transmission at the resonance wavelength are highlighted and the effects of index apodization and length apodization on the transmission spectra of multi-section LPFGs with zero- and π-phase shifts are illustrated with examples. We show that apodization can be employed effectively to suppress side lobes, or, in the other extreme, generate large, useful side lobes, as in the case of realizing a comb spectrum using a binary index apodization profile. Our results should be useful for the design of LPFG devices. We should point out that, it is difficult, if not impossible, to achieve a neat band-pass transmission spectrum with an LPFG, whether it contains

π-phase shifts or not, as an LPFG is a natural band-rejection filter. By using two parallel identical LPFGs [14,15], however, one can achieve a neat band-pass function through light coupling between the LPFGs and the coupling efficiency can, in principle, reach 100% [31].

Acknowledgement

This work was supported by a grant from the Research Grants Council of the Hong Kong Special Administrative Region, China [Project Number CityU 1041/99E].

References

[1] A.M. Vengsarkar, P.J. Lemaire, J.B. Judkins, V. Bhatia, T. Erdogan, J.E. Sipe, J. Lightwave Technol. 14 (1996) 58.
[2] A.M. Vengsarkar, J.R. Pedrazzani, J.B. Jukins, J.P. Lemaire, N.S. Bergano, C.R. Davidson, Opt. Lett. 21 (1996) 336.
[3] P.F. Wysocki, J.B. Judkins, R.P. Espindola, M. Andrejco, A.M. Vengsarkar, IEEE Photon. Technol. Lett. 9 (1997) 1343.
[4] J.R. Qian, H.F. Chen, Electron. Lett. 34 (1998) 1132.
[5] M.K. Pandit, K.S. Chiang, Z.H. Chen, S.P. Li, Microwave and Opt. Technol. Lett. 25 (2000) 181.
[6] M.K. Pandit, K.S. Chiang, S.P. Li, K.K. Cheung, Z. Chen, Microwave and Opt. Technol. Lett. 27 (2000) 419.
[7] O. Deparis, R. Kiyan, O. Pottiez, M. Blondel, Opt. Lett. 26 (2001) 1239.
[8] M. Harumoto, M. Shigehara, H. Suganuma, J. Lightwave Technol. 20 (2002) 1027.
[9] M. Das, K. Thyagarajan, Opt. Commun. 197 (2001) 67.
[10] D.B. Stegall, T. Erdogan, J. Opt. Soc. Am. A 17 (2000) 304.
[11] F. Ouellette, J.F. Cliche, S. Gagnon, J. Lightwave Technol. 12 (1994) 1728.
[12] A.A. Abramov, A. Hale, R.S. Windeler, T.A. Strasser, Electron. Lett. 35 (1999) 81.
[13] X. Shu, T. Allsop, B. Gwandu, L. Zhang, I. Bennion, IEEE Photon. Technol. Lett. 13 (2001) 818.
[14] K.S. Chiang, Y. Liu, M.N. Ng, S. Li, Electron. Lett. 36 (2000) 966.
[15] V. Grubsky, D.S. Starodubov, J. Feinberg, Tech. Digest Opt. Fiber Commun. Conf. 2000 4 (2000) 28.
[16] V. Bhatia, A.M. Vengsarkar, Opt. Lett. 21 (1996) 21.
[17] M.N. Ng, Z. Chen, K.S. Chiang, IEEE Photon. Technol. Lett. 14 (2002) 361.
[18] Y.J. Rao, Y.P. Wang, Z.L. Ran, T. Zhu, J. Lightwave Technol. 21 (2003) 1320.
[19] X. Yang, X. Guo, C. Lu, C.T. Hiang, Microw. Opt. Techn. Let. 35 (2002) 283.
[20] F. Bakhti, P. Sansonetti, J. Lightwave Technol. 15 (1997) 1433.
[21] H. Ke, K.S. Chiang, J.H. Peng, IEEE Photon. Technol. Lett. 10 (1998) 1596.
[22] L.R. Chen, Opt. Commun. 205 (2002) 271.
[23] J. Zhang, P. Shum, S.Y. Li, N.Q. Ngo, X.P. Cheng, J.H. Ng, IEEE Photon. Technol. Lett. 15 (2003) 1558.
[24] M. Miyagi, S. Nishida, J. Opt. Soc. Am. 69 (1979) 291.
[25] X.J. Gu, Opt. Lett. 23 (1998) 509.
[26] Y. Liu, J.A.R. Williams, L. Zhang, I. Bennion, Opt. Commun. 164 (1999) 27.
[27] Y. Jeong, S. Baek, B. Lee, IEEE Photon. Technol. Lett. 12 (2000) 1216.
[28] B.H. Lee, J. Nishii, Appl. Opt. 38 (1999) 3450.
[29] Y.G. Han, S.H. Kim, S.B. Lee, Opt. Express 12 (2004) 1902.
[30] B.O. Guan, A.P. Zhang, H.Y. Tam, H.L.W. Chan, C.L. Choy, X.M. Tao, M.S. Demokan, IEEE Photon. Technol. Lett. 14 (2002) 657.
[31] K.S. Chiang, F.Y.M. Chan, M.N. Ng, J. Lightwave Technol. 22 (2004) 1358.